Unlubricated Rolling and Sliding Wear Against Steel of Carbon-Black-Reinforced and *In Situ* Cured Polyurethane Containing Ethylene/Propylene/Diene Rubber Compounds

D. Xu,[1] J. Karger-Kocsis[2]

[1]*Institut für Verbundwerkstoffe GmbH, Kaiserslautern University of Technology, Erwin Schrödinger Strasse 58, 67663 Kaiserslautern, Germany*
[2]*Department of Polymer Technology, Faculty of Engineering and Built Environment, Tshwane University of Technology, Pretoria 0001, Republic of South Africa*

Received 4 December 2008; accepted 19 July 2009
DOI 10.1002/app.31156
Published online 7 October 2009 in Wiley InterScience (www.interscience.wiley.com).

ABSTRACT: The dry rolling and sliding friction and wear of ethylene/propylene/diene rubber containing carbon black and *in situ* cured polyurethane (EPDM+PUR_CB) were studied. For rolling and sliding tests against steel counterparts, different experimental conditions and tribotests were selected. The apparent network properties and phase structures of the rubbers were derived from dynamic mechanical thermal analysis and atomic force microscopy results. It was concluded that in EPDM+PUR_CB, both rubber phases, present in a 1 : 1 ratio, were continuous (interpenetrating network). The coefficient of friction (COF), specific wear rate (W_s), and heat development during the tribotests were determined. The carbon black and polyurethane contents did not much influence the COF in rolling wear tests. W_s of the ethylene/propylene/diene rubber containing carbon black went through a minimum as a function of the carbon black content. W_s of the EPDM+PUR_CB compounds decreased monotonously with an increasing amount of carbon black. The incorporation of polyurethane into the ethylene/propylene/diene rubber compounds decreased the resistance to rolling wear markedly. With carbon black filling of the ethylene/propylene/diene rubber–polyurethane compound, the COF and W_s increased and dramatically decreased, respectively, under sliding wear. The wear mechanisms were inspected with scanning electron microscopy and discussed as a function of recipe modifications and changes in the testing conditions. © 2009 Wiley Periodicals, Inc. J Appl Polym Sci 115: 1651–1662, 2010

Key words: interpenetrating networks (IPN); morphology; polyurethanes; rubber; structure–property relations

INTRODUCTION

Ethylene/propylene/diene rubber (EPDM) is a preferred rubber for many applications, including window seals, sealing rings, radiator seals, conveyor belts, and electrical insulation parts. Accordingly, a large body of scientific work is already devoted to the property modification of EPDM rubbers.[1–3]

Polyurethane (PUR) is applied in many different fields because of its excellent properties, including its wear resistance. Therefore, extensive research and development activity has addressed various aspects of the preparation and properties (e.g., mechanical and electrical properties) of PUR.[4–8] The sliding friction and wear characteristics are always preferred topics of PUR development.[9–14]

The favorable properties of the aforementioned rubbers have raised interest in combining them, that is, in developing rubber blends containing EPDM and PUR. This strategy has proved to be very promising. Sombatsompop[15] used PUR foam particles as reinforcing fillers in EPDM mixes. His results showed that the compounds exhibited optimum dynamic mechanical properties when PUR particles [30 part per hundred part rubber (phr)] were incorporated into EPDM. The morphology development, mechanical properties, rheology, and compatibility of EPDM and thermoplastic PUR blends were studied by Wang and coworkers[16,17] and Dhamodharan et al.[18] The aforementioned methods, that is, filling with ground PUR and blending with thermoplastic PUR, have limitations because the modified rubbers lose their rubbery characteristics. Therefore, it is of great importance to find alternative methods for rubber/PUR combinations.

Thermoset PUR/rubber compounds are scarcely reported in the literature. However, such compounds can be produced in a very elegant way. PUR precursors, ready to be crosslinked *in situ*, are available also in a solid form, which is strongly favored in rubber compounding. These precursors usually contain crystalline polyols and blocked polyisocyanates. Above the deblocking temperature of the

Correspondence to: J. Karger-Kocsis (karger@pt.bme.hu).

latter compound, a crosslinked (thermoset) PUR can be produced *in situ*. Because the deblocking temperature of the polyisocyanate is below the usual curing temperature of rubbers, various thermoset PUR/rubber combinations can be generated. The beauty of this approach is that the crosslinking reactions of such PURs and rubbers are very different, and thus between them, no interference is expected. This strategy has not yet been followed in the open literature to the best of our knowledge.

The aim of this work was to prove the feasibility of this blending route for a polar (PUR)–apolar (EPDM) rubber combination. A further aim was to check whether the corresponding compounds exhibited improved resistance to rolling and sliding wear. Therefore, carbon black (CB) containing compounds of EPDM and EPDM and PUR (1 : 1 w/w; denoted EPDM+PUR) were studied with respect to their dry rolling and sliding friction and wear performance under different experimental conditions. Tests were performed in orbital rolling ball (steel)-on-plate (rubber; orbital-RBOP), pin (steel)-on-plate (rubber; POP), roller (steel)-on-plate (rubber; ROP), and oscillating cylinder (steel)-on-plate (rubber; fretting) testing configurations without lubrication. Dynamic mechanical thermal analysis (DMTA) and atomic force microscopy (AFM) were adopted to get information on the phase structures of the rubber compounds. The coefficient of friction (COF) and the specific wear rate (W_s) were determined. The wear mechanisms were deduced by an inspection of the worn surfaces with scanning electron microscopy (SEM) and discussed as a function of the recipe and testing conditions.

EXPERIMENTAL

Materials and sample preparation

EPDM rubbers

The recipe used was as follows: 100 parts EPDM (Keltan 512, DSM Elastomers, Sittard, The Netherlands); 0, 30, 45, or 60 parts CB (N550); 5 parts ZnO; 1 part stearic acid, 1.5 parts sulfur; 0.6 parts *N*-cyclohexyl-2-benzothiazole sulfenamide (Vulkacit CZ, Bayer, Leverkusen, Germany); 0.6 parts 2-mercaptobenzothiazole (Vulkacit Mercapto, Bayer); 0.6 parts zinc dicyanatodiamine (Rhenogran Geniplex 80, Rhein Chemie, Mannheim, Germany); and 1.5 parts zinc dibenzyl dithiocarbamate (Rhenogran ZBEC-70, Rhein Chemie). The CB content was varied from 0 to 60 phr. Rubber sheets (ca. 2 mm thick) were produced by compression molding at 170°C and 7 MPa with a press from Weber (Remshalden, Germany) for 12 min. The vulcanization time was adjusted by the consideration of the time needed for 90% crosslinking at a temperature of 170°C. The related time was read from Monsanto moving-die rheometer (MDR 2000 EA-1; Alpha Technologies, Swindon, UK) curves. These EPDM rubbers are denoted as follows: EPDM_0, EPDM_30, EPDM_45, and EPDM_60 (where the digits in the designations represent the CB content in phr).

EPDM+PUR compounds

The EPDM+PUR compounds were produced by the dilution of the previous ready-to-cure EPDM rubbers with PUR with an EPDM/PUR ratio of 1 : 1. An *in situ* crosslinkable PUR powder (Collano HCM 555-D, Nolax AG, Sempach-Station, Switzerland) was used that contained solid polyol and solid blocked polyisocyanate. This PUR, available in a fine powder form, was incorporated into the previously prepared EPDM mixes on a laboratory two-roll mixing mill (LRM-150/3E, Labtech, Bangkok, Thailand) at a temperature of about 30°C with a friction ratio of about 1.4. Deblocking and crosslinking of the PUR occurred under the vulcanization conditions selected for the EPDM (discussed previously). The PUR powder was already cured when the temperature reached 150°C according to differential scanning calorimetry results.[19] PUR was incorporated into EPDM_CB in a 1 : 1 ratio, with the original CB content reduced by half. This is the reason for the designations introduced: EPDM+PUR_0, EPDM+PUR_15, EPDM+PUR_22.5, and EPDM+PUR_30. Again, the two last digits refer to the CB content in the corresponding EPDM+PUR compounds in phr units.

Characterization

Phase structure

To get a deeper insight into the structure of EPDM_CB and EPDM+PUR_CB, the related systems were subjected to DMTA and AFM investigations.

DMTA spectra were measured on rectangular specimens in a tensile mode with a constant strain of 0.01% as a function of temperature (from −100 to +100°C) with a frequency of 1 Hz with a Q800 device from TA Instruments (New Castle, DE). From −100°C, the temperature was increased in 5°C steps, and at each step, the temperature was stabilized for 3 min.

AFM analysis was performed in a tapping mode with a scanning probe microscope system (Veeco, Santa Barbara, CA). The Si-tipped cantilever (length = 250 μm, spring constant ~ 20 N/m) was operated at a resonant frequency of approximately 350 MHz during the scanning. Phase images were taken from the torn and cut surfaces of the EPDM and EPDM+PUR, respectively. Tearing was carried out by hand after a cut was made on the edge of the specimen with a clean razor blade. Cutting was performed with a clean, sharp blade. The AFM scans were executed

immediately after the torn or cut surfaces of the compounds were produced.

Density and hardness

The density and Martens hardness (HM) of the compounds were determined. The density was assessed with Archimedes' principle (the buoyancy method with water) according to the ISO 1183 standard. The HM was measured according to the ISO 14577-1 standard (2002) with a Shimadzu DUH 202 device from Shimadzu Corp. (Kyoto, Japan) equipped with a Vickers-type diamond indenter. The hardness was determined at a maximum force of 5 mN after a holding time of 2 s.

Rolling and sliding wear tests

Rolling wear. To evaluate the rolling friction and wear of the rubber compounds, a homemade orbital-RBOP test rig was used. In this rig, a steel ball [100Cr6; diameter = 14 mm, arithmetical roughness (R_a) = 1 μm] was rolled along a circular path (diameter = 33 mm) on a rubber sheet. The steel ball was pushed by a defined normal load against the rubber sheet. The parameters set for this configuration were a normal load of 90 N, a speed of 280 rpm, and a duration of 3 h. This device allowed us to record the COF as a function of time. The wear rate and wear mechanisms were determined as described in the section on sliding wear.

The temperature development on the worn surfaces during the first hour of testing was surveyed with an infrared thermal camera (InfraTec, Dresden, Germany).

Sliding wear. Sliding friction and wear characteristics were assessed with POP, ROP, and fretting tribotests under dry conditions.

In the POP tests, a device from Wazau (Berlin, Germany) was used in which a steel pin (100Cr6; $R_a < 1$ μm) with a hemispherical head 10 mm in diameter rotated along a circular path 33 mm in diameter. The pin was pressed to the rubber plate with a given load. The following parameters were chosen for this configuration: a normal load of 2 N, a sliding speed of 250 mm/s, and a duration of 90 min.

In the ROP tests, a self-rotating steel roller (9SMnPb28k; diameter = 10 mm, width = 20 mm, $R_a \approx 0.9$ μm) was pressed against a rubber strip 8 mm wide in an SOP 3000 tribotester (Dr Tillwich GmbH, Horb-Ahldorf, Germany). The test parameters were as follows: a load of 4 N, a sliding speed of 250 mm/s, and a duration of 90 min.

In the third tribotest (fretting), an oscillating steel cylinder was pressed against a fixed rubber specimen by a defined normal load. The diameter and contact length of the cylinder ($R_a \approx 0.9$ μm) were 15 and 10 mm, respectively. The applied experimental parameters were a normal load of 10 N, an oscillation frequency of 10 Hz, a stroke of 3 mm, and a duration of 90 min.

All these test rigs allowed us to monitor the dynamic COF as a function of time (i.e., the sliding distance).

W_s was calculated as follows:

$$W_s = \frac{\Delta V}{FL} \tag{1}$$

where ΔV is the loss volume (mm^3), F is the normal load (N), and L is the overall rolling/sliding distance (m). ΔV was calculated by the measurement of the depth and width of the wear tracks by a white light profilometer (shown later) under the assumption that the shape of the wear track was a half-ellipse.

The test setup for the aforementioned testing methods is depicted schematically in Figure 1.

The worn surfaces were inspected with a Micro-Prof white light profilometer (Fries Research & Technology, Bergisch Gladbach, Germany) and with SEM (JSM-6300, JEOL, Japan), respectively. Before the SEM investigation at high acceleration voltages, the specimens were sputtered with a gold/palladium alloy with a device from Balzers (Liechtenstein).

RESULTS AND DISCUSSION

Phase structure

Figure 2 displays the course of the storage modulus (E') and loss factor (tan δ) as functions of the temperature (−100 to 100°C). With increasing CB reinforcement, the stiffness (E') increases in the whole temperature range for both EPDM [cf. Fig. 2(a)] and EPDM+PUR-based systems [cf. Fig. 2(b)]. The monotonous decrease of tan δ with increasing CB content in the EPDM mixes well reflects the content and reinforcing effect of CB. The glass-transition temperature (T_g) of EPDM is about −45°C. Above this T_g, the plateau modulus (E_{pl}) of the EPDM_CB compounds is very pronounced in the semilogarithmic plot. E_{pl} increases with increasing CB content and at the same time becomes less constant with increasing temperature, as expected.

The DMTA spectra of the EPDM+PUR_CB system differ markedly in the rubbery state from those of EPDM_CB. T_g (≈ −50°C) of this PUR is closely matched to that of EPDM.[19] Because of the small difference between the related T_g values, the mechanical loss peak at a temperature of −45°C broadens (cf. the related section about tan δ–temperature traces in Fig. 2(a,b)]. The other fundamental difference between EPDM_CB and EPDM+PUR_CB is linked to a rubbery plateau just above the T_g values of PUR and EPDM. E_{pl} is much higher in

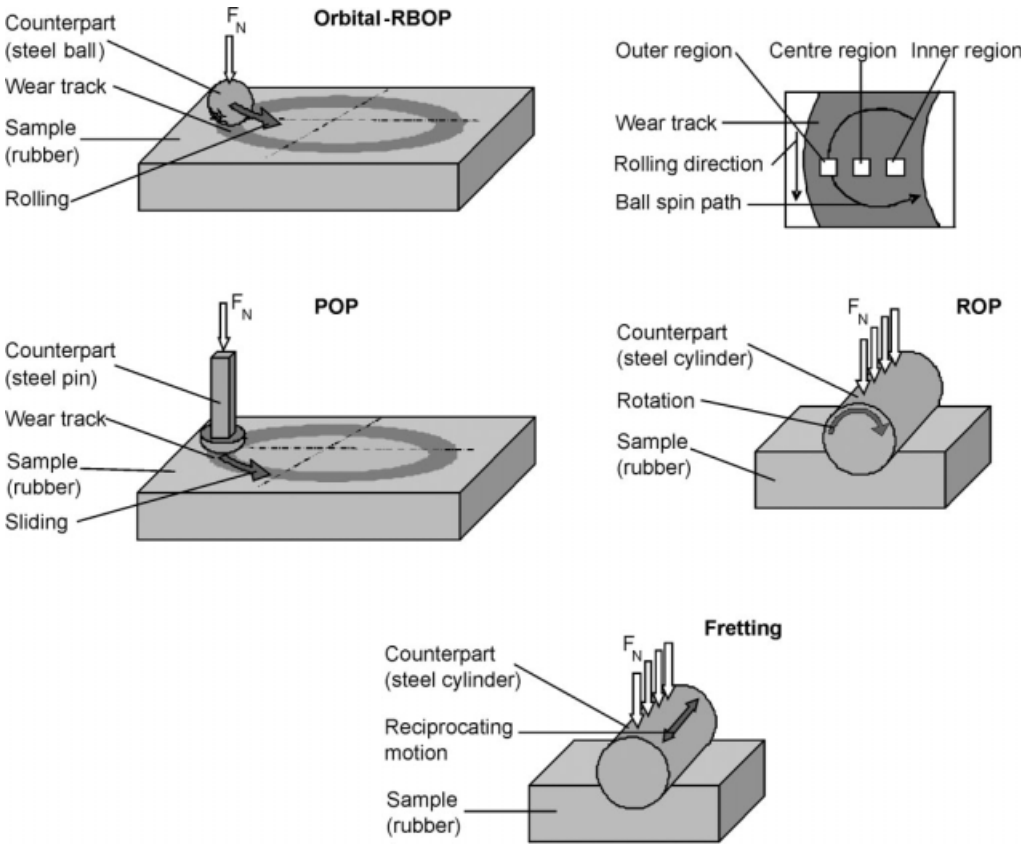

Figure 1 Schemes of the test configurations of orbital-RBOP, POP, ROP, and fretting. This figure also shows the preparation of the samples for SEM investigations after orbital-RBOP testing (top right).

EPDM+PUR_CB than in EPDM_CB. Moreover, the plateau is far less pronounced for EPDM+PUR_CB than for EPDM_CB. The decreasing E_{pl} value with the temperature suggests that this PUR has some thermoplastic component. This is linked with the soft phase of this PUR, which melts at about 50°C.[19] This melting is obvious in both E'–temperature and tan δ–temperature traces in Figure 2(b). The sharp drop in E' at about 50°C along with the extremely high E_{pl} values in the temperature range of −40 to 50°C for EPDM+PUR_CB clearly suggests that both PUR and EPDM are continuous phases. Accordingly, an interpenetrating network (IPN) structure has been formed.

According to the rubber elasticity theory, the inverse of the plateau modulus ($1/E_{pl}$) at temperatures above T_g correlates with the mean molecular mass between crosslinks (M_c):

$$E_{pl} = \frac{3\rho RT}{M_c} \tag{2}$$

where E_{pl} is the modulus (in this context at 298 K), ρ is the density, R is the universal gas constant (8.314 J K^{-1}·mol^{-1}), and T is the absolute temperature.

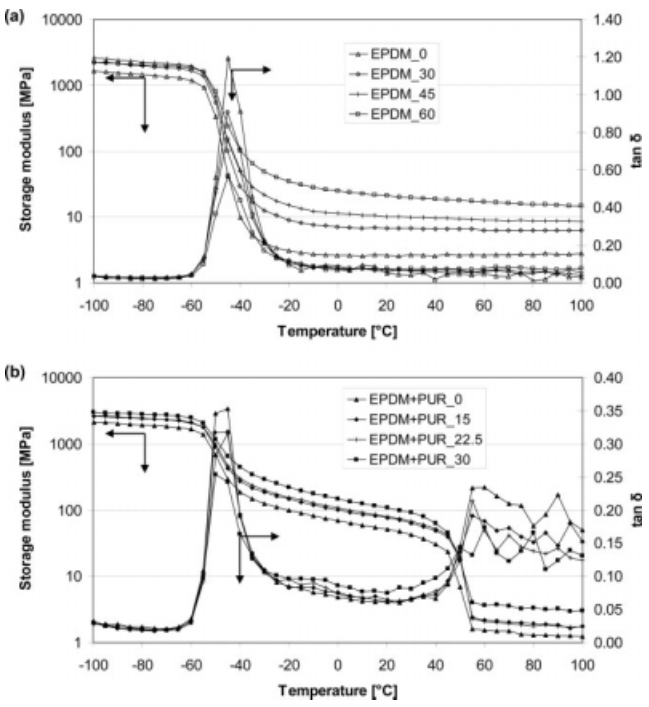

Figure 2 E' and tan δ versus temperature traces for the (a) EPDM_CB and (b) EPDM+PUR_CB compounds.

TABLE I
Basic Network-Related and Mechanical Properties of the EPDM and EPDM+PUR Rubbers

Property	EPDM_0	EPDM_30	EPDM_45	EPDM_60
Density (g/cm^3)	0.922	1.026	1.021	1.097
Tan δ at T_g (−45°C)	1.193	0.907	0.765	0.570
M_c (g/mol; 25°C)	2707	1149	759	403
v_c (mol/m^3)	340	892	1345	2722
HM (MPa)	0.6	2.1	2.3	3.0
Property	EPDM+PUR_0	EPDM+PUR_15	EPDM+PUR_22.5	EPDM+PUR_30
Density (g/cm^3)	0.996	1.063	1.063	1.114
Tan δ at T_g (−45°C)	0.353	0.318	0.315	0.242
M_c (g/mol; 25°C)	156	113	106	83
v_c (mol/m^3)	6,369	9,448	10,019	13,426

It is more straightforward to consider the apparent network density (v_c):

$$v_c = \frac{\rho}{M_c} \tag{3}$$

Both M_c and v_c are apparent values. *Apparent* means that not only chemical crosslinking but also rubber–CB, CB–CB, and, in the case of EPDM+PUR_CB, IPN-type interactions are involved in the corresponding terms. The network-related data are summarized in Table I. We can recognize that M_c decreases and thus v_c increases with increasing CB content for both rubber systems. M_c and v_c of EPDM are greater and less, respectively, than those of EPDM+PUR.

Figure 3(a) shows the AFM phase image of EPDM_60, displaying a sea-island structure. The agglomerated CB appears as a dark phase in the EPDM matrix. For EPDM+PUR_CB, the phase structure basically changes. There are two different types of structures: a sea-island morphology (as before) and a cocontinuous (IPN) morphology. The IPN structuring becomes obvious at a lower magnification, suggesting that the EPDM and PUR phases are coarsely intermingled [cf. Fig. 3(b)]. This is supported by the polarity difference between EPDM and PUR as well as their ratio (viz. 1 : 1) setting. Therefore, the AFM observations are in line with the DMTA results, supporting the idea that EPDM and PUR are immiscible and that both form quasicontinuous phases. The magnified image from position c in Figure 3(b) is depicted in Figure 3(c). It shows the same characteristics as Figure 3(a) taken from EPDM_60. Therefore, it corresponds to the component of EPDM_CB. Figure 3(b,c) suggests at the same time that CB remained completely in the EPDM phase. Recall that during the preparation of EPDM+PUR_CB, the EPDM_CB mixes were diluted by *in situ* polymerizable and crosslinkable PUR. This mixing procedure favors the idea that no CB partitioning occurs between the EPDM and PUR phases, which are, in addition, highly apolar and polar, respectively.

Physicomechanical properties

Table I also shows that CB enhances the density of both EPDM and EPDM+PUR materials. The HM of

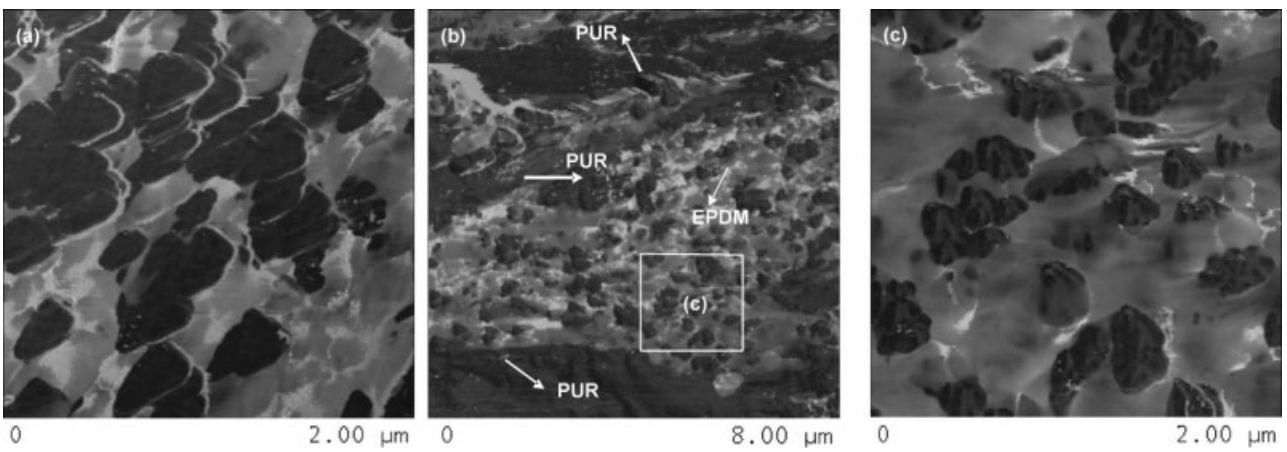

Figure 3 AFM images of the (a, torn surface) EPDM_60 and (b,c, cut surface) EPDM+PUR_30.

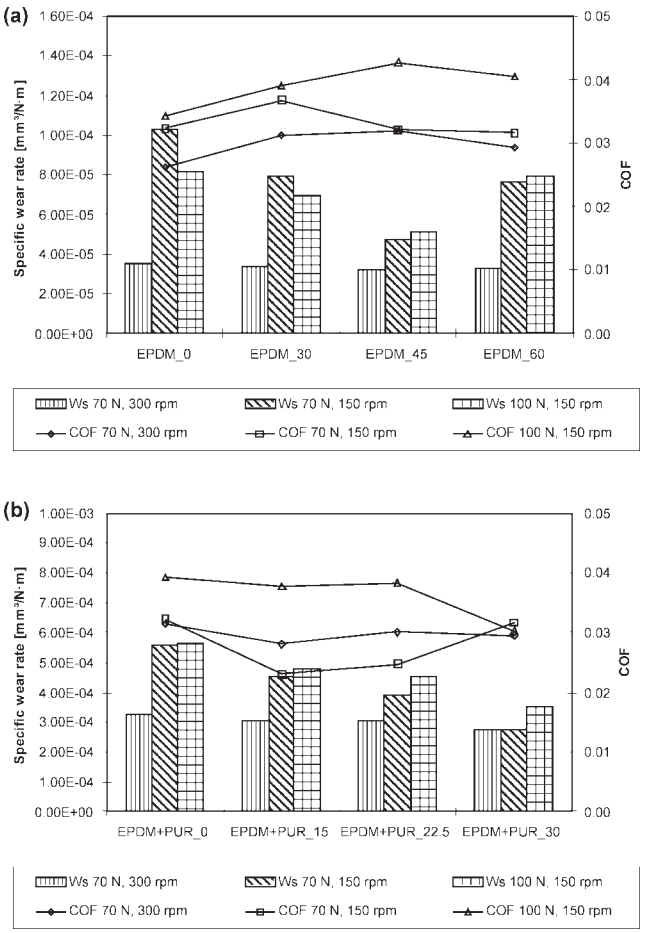

Figure 4 Changes in COF (line) and W_s (column) for the (a) EPDM_CB and (b) EPDM+PUR_CB compounds in orbital-RBOP testing.

EPDM increases with increasing CB content. The HM values of the EPDM+PUR systems show large scattering. This can be attributed to the presence of the IPN structures of these compounds and thus is not reported in Table I.

Rolling friction and wear

The COF and W_s values measured for EPDM_CB and EPDM+PUR_CB under different experimental conditions in the orbital-RBOP configuration are summarized in Figure 4. Note that the incorporation of CB has a marginal effect on the COF of both types of rubber mixes. Furthermore, the difference in the COF between the EPDM and EPDM+PUR-based systems is very small under the same testing conditions. W_s of the EPDM_CB rubbers goes through a minimum as a function of the CB content. The incorporation of 45 phr CB into EPDM resulted in the smallest W_s value in comparison with the other EPDM_CB rubbers under the selected experimental conditions. W_s of EPDM+PUR_CB decreased monotonously with an increasing content of CB. For both rubber systems, the tests under 70 N and 300 rpm yielded the lowest W_s values. This was due to the doubling of the rolling distance in comparison with the tests performed at 150 rpm. Note that the rolling distance is in the denominator of eq. (1), which was used to calculate W_s. The increase in the normal load increased W_s monotonously for EPDM+PUR but decreased it for EPDM rubbers. However, the incorporation of PUR into the EPDM compounds decreased the resistance to rolling wear markedly [cf. Fig. 4(a,b)]. This suggests that the development of an IPN structure (at least without chemical interactions between its constituents) is not beneficial for improving the resistance to rolling wear.

SEM pictures taken from the worn surfaces of selected EPDM_CB compounds tested under 70 N and 300 rpm in the orbital-RBOP configuration are shown in Figures 5–7. Because the ball in the test setup is led by a bearing ring fixed at a motor shaft, it rotates with concentric revolutions and spins at the same time (cf. Fig. 1). As a result, the wear

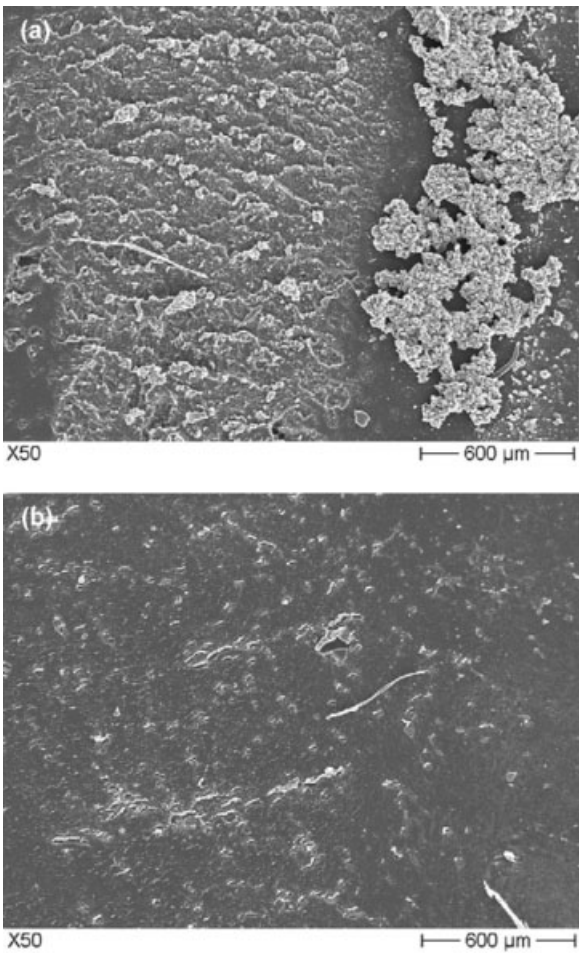

Figure 5 SEM pictures taken from the rolling wear track of EPDM_0 after orbital-RBOP testing under 70 N and 300 rpm: (a) outer region and (b) inner region (note that the rolling direction was downward).

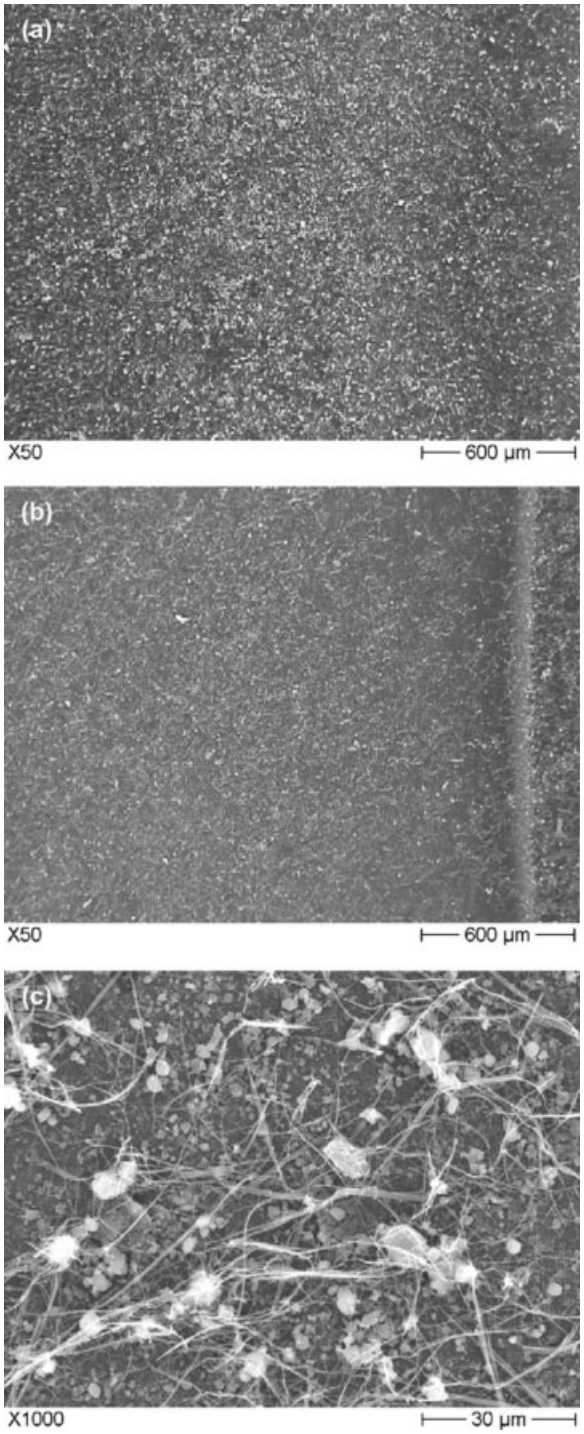

Figure 6 SEM pictures taken from the rolling wear track of EPDM_45 after orbital-RBOP testing under 70 N and 300 rpm: (a) outer region, (b) inner region, and (c) detail from the central region (note that rolling direction was downward).

mechanisms may be different along the width of the wear track. This is the reason for the sampling from three regions[20] (cf. the sampling sketch in Fig. 1, top right). Figure 5 shows the wear track of EPDM_0 at 70 N and 300 rpm. Figure 5(a,b) originates from the regions with additional forward (outer region, cf. Fig. 1) and backward spin of the ball (inner region, cf. Fig. 1), respectively. A Schallamach-type pattern can be recognized in the outer region. This is due to the buckling of the rubber as a result of elastic instability attributable to tangential compressive stresses in the contact area.[21] Holes, rollers, scratches, and a

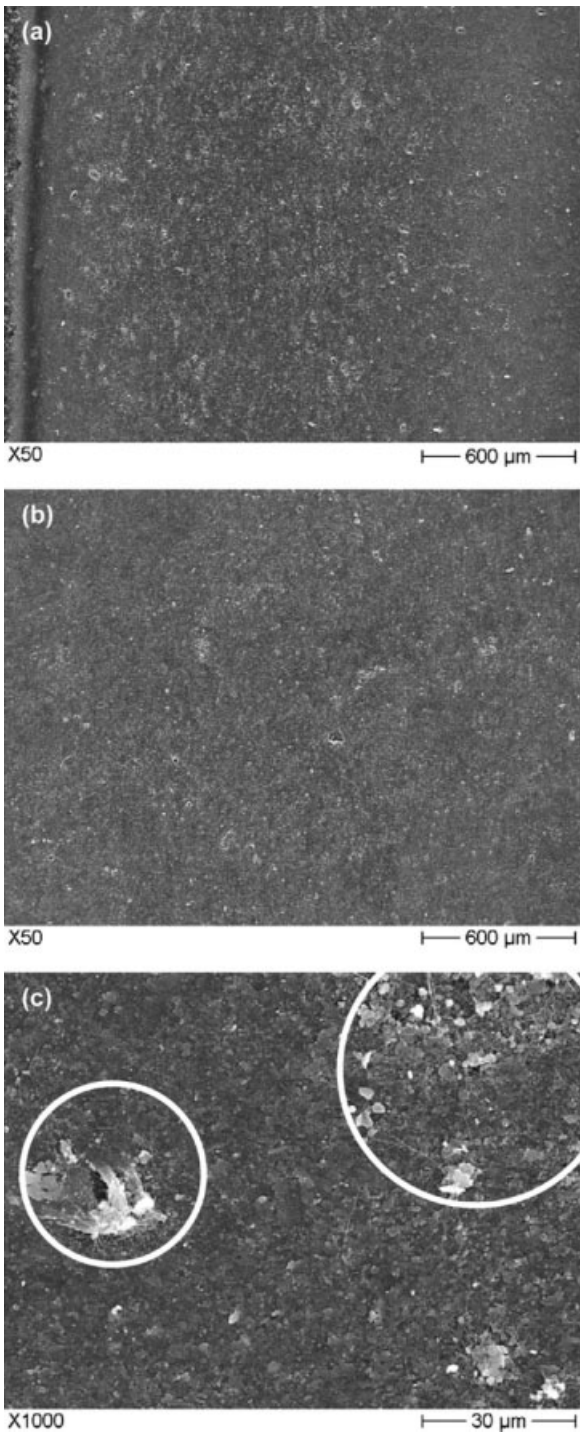

Figure 7 SEM pictures taken from the rolling wear track of EPDM_60 after orbital-RBOP testing under 70 N and 300 rpm: (a) outer region, (b) inner region, and (c) detail from the central region (note that the rolling direction was downward).

few fibrils can be seen in the inner region [cf. Fig. 5(b)].

The incorporation of CB changed the wear characteristics in comparison with those of the neat EPDM (cf. Figs. 6 and 7). The wear track of EPDM_45 is dominated by the formation of particles and fibrils observable at a high magnification [cf. Fig. 6(c)].

The COF and W_s of EPDM_60 did not fit the expected tendency, that is, monotonously changing with an increasing amount of CB [cf. Fig. 4(a)]. The W_s values for EPDM_60 under all experimental conditions were higher than those of EPDM_45 and even EPDM_30 under the testing conditions of 100 N and 150 rpm [cf. Fig. 4(a)]. The SEM pictures from the wear track of EPDM_60 are shown in Figure 7. Holes and flattened fibrils can be observed in the three regions of the worn surface. The former suggests considerable fatigue-type damage, which may account for the unusually higher W_s values of EPDM_60 in comparison with the other EPDM_CB compounds.

The wear mechanisms of the EPDM_CB compounds under the testing conditions of 70 N and 150 rpm and 100 N and 150 rpm were very similar to those under the testing conditions of 70 N and 300 rpm, although some changes could be resolved by high-magnification SEM inspection. These changes were related to the density of the roll and hole developments, the distance between the neighboring Schallamach waves, and the like.

Figure 8 shows the worn surface of EPDM+PUR_0. The formation of agglomerates, including rolls, is the basic wear mechanism. This accounts for the much higher W_s values versus those of the corresponding EPDM_0. Moreover, the agglomerates in the three regions (cf. Fig. 1) have different shapes: rolls in the outer region, ironed agglomerates in the center region, and no distinctly shaped debris in the inner region. This reflects again the differences in the velocity profile of the ball in different regions of the wear track. Note that the effect of ball spin in the outer region of the worn track is more prominent than in the inner one.

The incorporation of CB reduced the tendency to form agglomerates during rolling wear of the compound EPDM+PUR_30 (cf. Fig. 9). Agglomerates could be discerned only in the center and inner regions of the worn surface. This is likely the explanation for the smaller W_s values versus those of EPDM+PUR_0. The different topography of the agglomerates in Figure 9 again reflects the effect of the spin of the steel ball.

The lower resistance to rolling wear of EPDM+PUR versus EPDM is contrary to expectations. The reason for this behavior is the IPN morphology without chemical interactions between the two phases within it. Therefore, EPDM+PUR is less resistant to rolling wear than EPDM. Thus, it would be of great relevance to trigger chemical interactions between EPDM and PUR, and maleated EPDM rubbers seem to be suitable candidates. Just as for EPDM_CB, the changes in the experimental

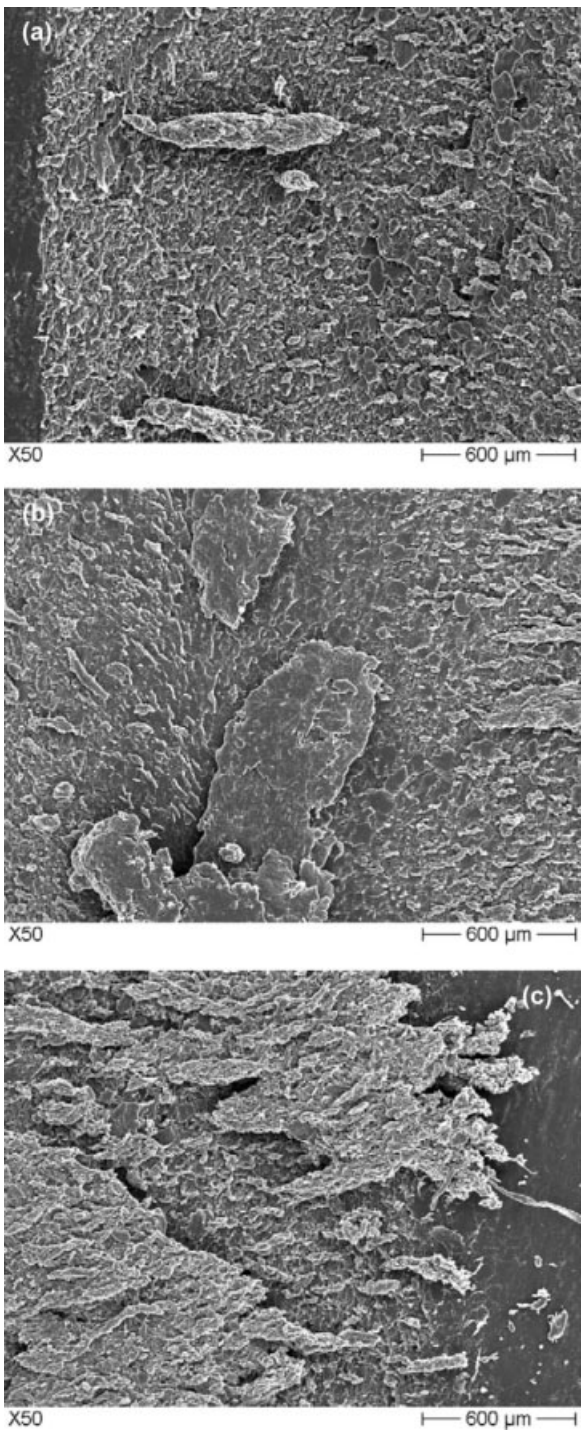

Figure 8 SEM pictures taken from the rolling wear track of EPDM+PUR_0 after orbital-RBOP testing under 70 N and 300 rpm: (a) outer region, (b) center region, and (c) inner region (note that the rolling direction was downward).

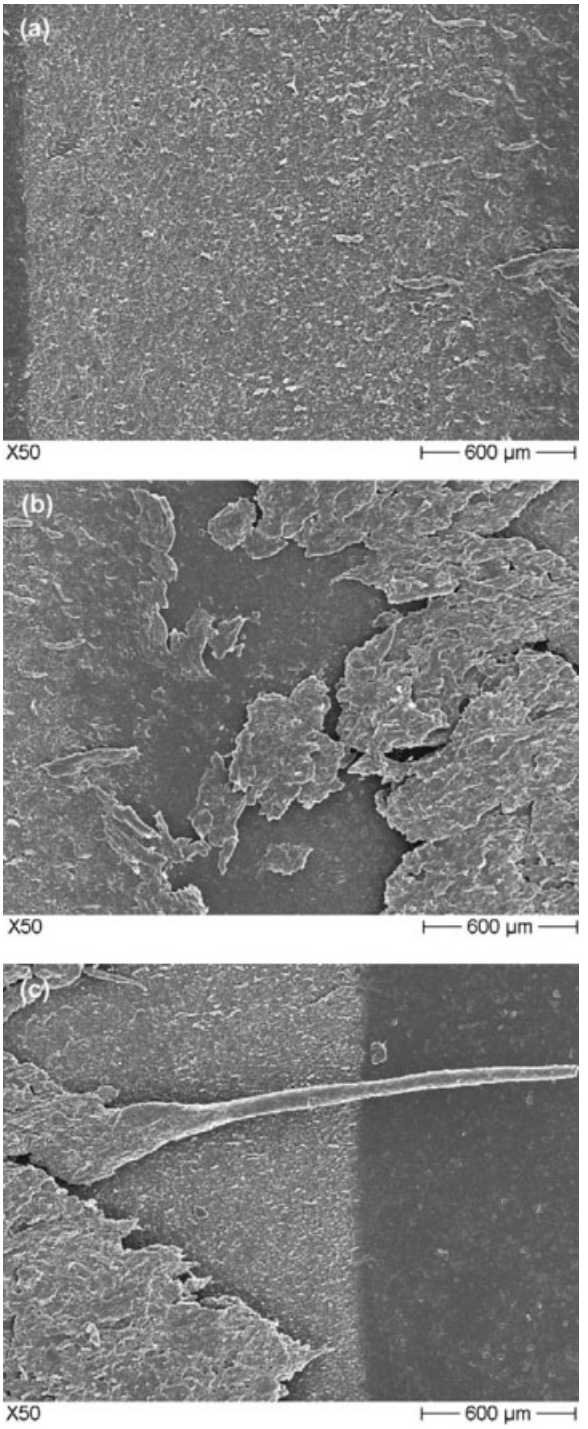

Figure 9 SEM pictures taken from the rolling wear track of EPDM+PUR_30 after orbital-RBOP testing under 70 N and 300 rpm: (a) outer region, (b) center region, and (c) inner region (note that the rolling direction was downward).

conditions did not affect the wear mechanisms of EPDM+PUR_CB markedly.

Figure 10(a) shows the temperature development within 1 h of the orbital-RBOP testing of EPDM_0 under 70 N and 300 rpm, 70 N and 150 rpm, and 100 N and 150 rpm, whereas in Figure 10(b), selected heat development traces, registered under 70 N and 150 rpm on EPDM_CB (EPDM_0 and EPDM_60) and EPDM+PUR_CB (EPDM+PUR_0 and EPDM+PUR_30) compounds, are collated. We can observe that the temperature development process can be divided into two stages: a fast-rising one (0–3 min) and a slow-rising one (3–60 min). The temperature rise for testing at 70 N and 150 rpm, 100 N and 150 rpm, and 70 N and 300 rpm was 1.6, 2 (at 30 min), and 3°C, respectively [cf. Fig. 10(a)]. Increases in both the normal load and ball speed enhanced the heat development. Note that with increasing normal force, the friction force increased as well [cf. Fig. 10(a)]. Furthermore, the COF is basically higher at a higher normal load, being the ratio of the friction force to the normal one. Therefore, more heat was generated in the tests performed at a higher normal load. With the doubling of the revolutions (speed) of the steel ball, the contact time at a given position on the surface of the sample was also doubled. In this case, the temperature rise was also approximately doubled, as demonstrated by the corresponding trace in Figure 10(a).

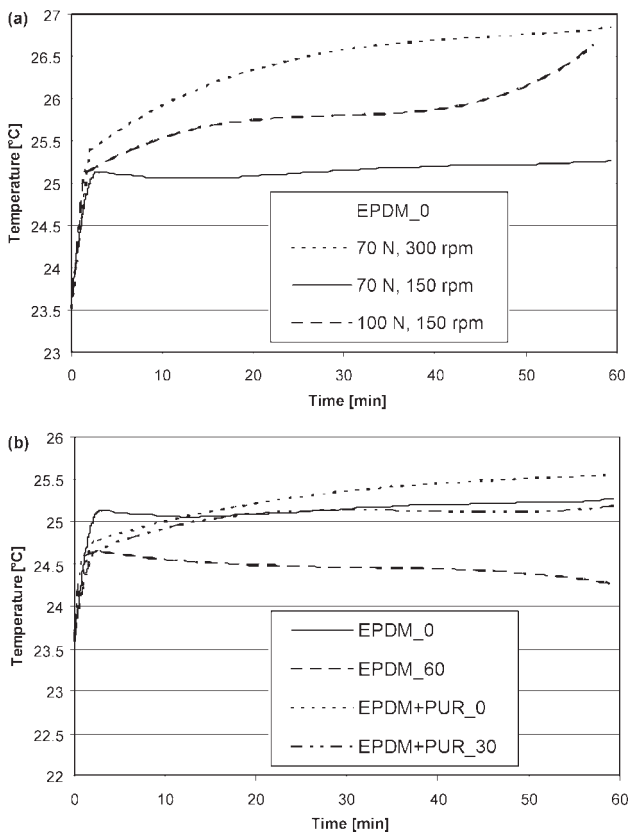

Figure 10 (a) Temperature development for EPDM_0 under the three experimental conditions in orbital-RBOP testing. (b) Temperature development for EPDM_0, EPDM_60, EPDM+PUR_0, and EPDM+PUR_30 under 70 N and 150 rpm in orbital-RBOP testing.

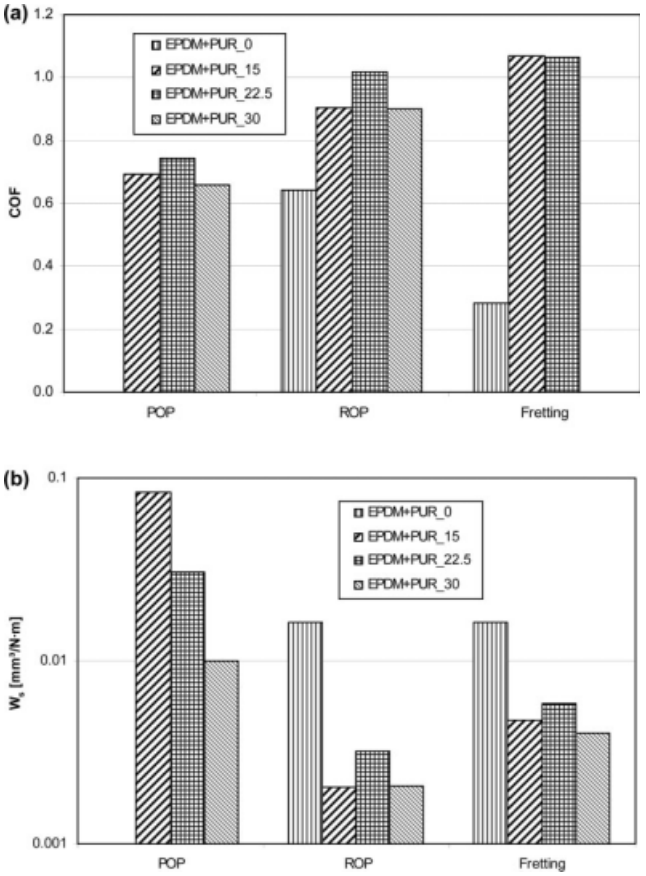

Figure 11 Steady-state dynamic (a) COF and (b) W_s of EPDM+PUR_CB after POP, ROP, and fretting tests.

Effects of CB and PUR incorporation on the heat development are shown in Figure 10(b). The addition of CB and PUR did not affect the two-stage heat-rising mode. Filling with CB decreased the temperature rise in 1 h. However, the incorporation of PUR enhanced the temperature rise in comparison with the corresponding EPDM_CB mixes. Heat generation in filled rubber vulcanizates is a complex issue, affected by the operating conditions and properties of the rubber at the same time. With respect to material properties, the heat generation increases with the hysteresis loss, specific heat, filler loading, and surface area of the filler increasing and decreases with the thermal conductivity, modulus, and structure of the filler increasing.[22] As the experiments were carried out practically under the same conditions, the difference in the temperature rise was mainly caused by the changes in the material properties induced by the incorporation of CB and PUR. When CB was added, the hysteresis loss, filler loading, thermal conductivity, and modulus increased; that is, adverse factors acted simultaneously. The measured temperature curves suggest that the latter two factors (i.e., increases in the thermal conductivity and stiffness) overwhelmed the former ones. PUR is no active filler for rubber; therefore, its effect on the heat generation needs further investigation. For EPDM_0 and EPDM_60, small temperature peaks separated the fast temperature-rising stage from the slow temperature-rising stage. When PUR was added, the temperature increased monotonously after the fast stage until the temperature stabilized during the test.

Sliding friction and wear

As sliding friction and wear results for EPDM_CB have been reported earlier,[23] here we focus only on the EPDM+PUR_CB system.

The unlubricated steady-state dynamic COF and W_s data for EPDM+PUR after POP, ROP, and fretting testing are shown in Figure 11. There are no W_s or COF data for EPDM+PUR_0 under POP because

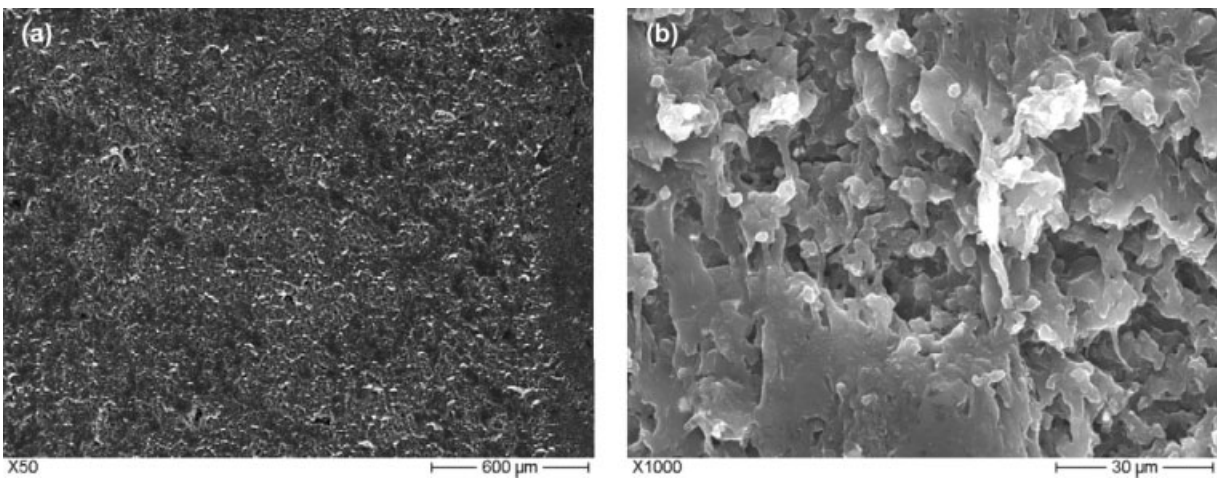

Figure 12 SEM pictures taken from the sliding wear track of EPDM+PUR_30 after POP testing (note that the sliding direction was downward).

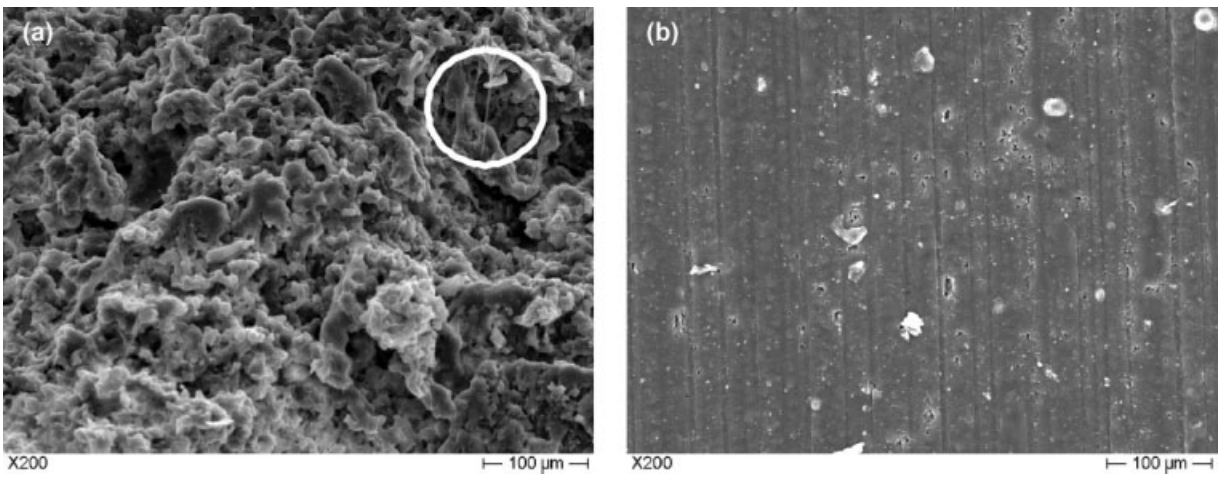

Figure 13 SEM pictures taken from the sliding wear tracks of (a) EPDM+PUR_0 and (b) EPDM+PUR_30 after ROP testing (note that the sliding direction was downward).

the samples were worn out during these tests. The COF value of EPDM+PUR_30 is missing because it was larger than 1.5 and could not be recorded by the fretting machine used. The COF and W_s values increased and dramatically decreased, respectively, with CB filling of EPDM+PUR (cf. Fig. 11).

SEM pictures taken from the worn surfaces of EPDM+PUR after POP, ROP, and fretting testing are collected in Figures 12–14. Note that there are no photographs for EPDM+PUR_0 because the sample was worn out, as stated before.

Figure 12 displays SEM pictures of EPDM+PUR_30 after POP testing. Fragmentation is the main wear mechanism for this system. Fragmentation is triggered by dense cracking, which is supported by the IPN-like structure of EPDM+PUR_CB.

In ROP tests, EPDM+PUR_0 and EPDM+PUR_30 were worn by fragmentation with very few fibrils [cf. Fig. 13(a)] and fatigue-induced surface cracking with hole formation [cf. Fig. 13(b)], respectively.

The worn surfaces of EPDM+PUR_0 and EPDM+PUR_30 after fretting tests are shown in Figure 14. Fragmentation is the wear characteristic for EPDM+PUR_0 [cf. Fig. 14(a)]. Ironed rollers with fatigue-induced holes can be observed in the fretting wear track of EPDM+PUR_30 [cf. Fig. 14(b)].

The SEM pictures confirm that under sliding conditions, ROP is the most severe test. It is worth noting that the worn surface topology of EPDM+PUR_0 suggests also the presence of an IPN structure [cf. especially Figs. 13(a) and 14(a)].

CONCLUSIONS

On the basis of this work devoted to studying the effects of CB and *in situ* cured PUR on the network-

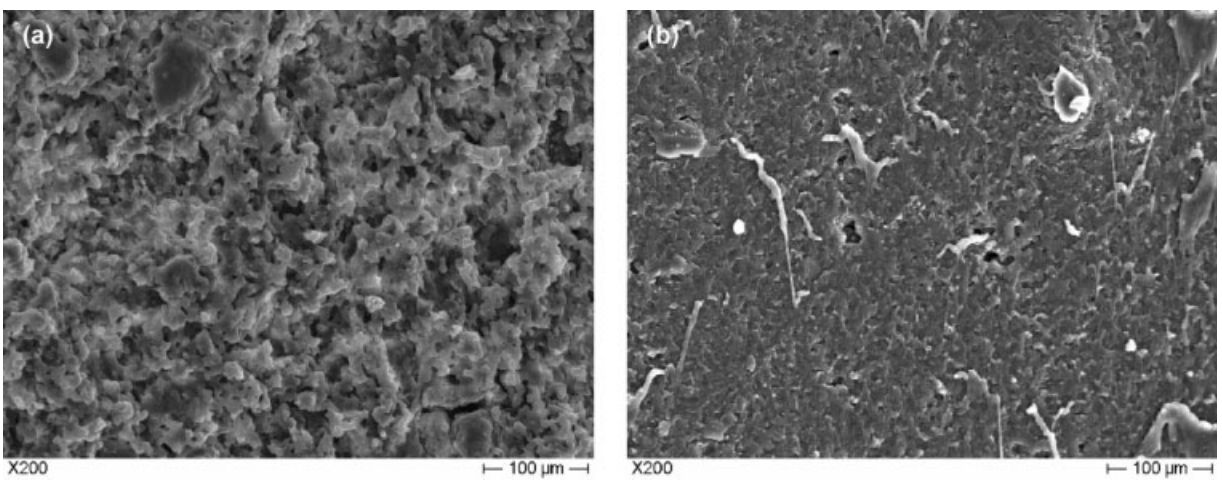

Figure 14 SEM pictures taken from the sliding wear tracks of (a) EPDM+PUR_0 and (b) EPDM+PUR_30 after fretting tests (note that the sliding direction was vertical).

related properties, phase structure, dry rolling, and sliding wear performance of sulfur-cured EPDM mixes, the following conclusions can be drawn:

The incorporation of CB and PUR increased the stiffness (E') of the mixes in their rubbery stage. The EPDM and PUR were fully incompatible and formed an IPN structure in the compounds according to DMTA and AFM results.

For rolling wear, CB and PUR did not much influence the COF under different experimental conditions. W_s of the EPDM_CB rubbers went through a minimum with the CB content. CB filling decreased the W_s values for EPDM+PUR-based rubbers. However, the incorporation of PUR into the EPDM compounds decreased the resistance to rolling wear markedly. This was attributed to the IPN structure present. The temperature development followed a two-stage process composed of a fast-rising stage (0–3 min) and a slow-rising stage (3–60 min). The increase in both the normal load and ball rolling speed increased the heat development.

For sliding wear, the COF and W_s values increased and dramatically decreased, respectively, with CB filling of the EPDM+PUR system.

One of the authors (D.X.) thanks the German Research Foundation for her fellowship within the graduate school (GK 814). This study was done in the framework of a bilateral collaboration between Slovenia and Hungary. The authors are thankful to Nolax AG (Sempach-Station, Switzerland) for providing the PUR material.

References

1. Slusarski, L.; Bielinski, D. M.; Affrossman, S.; Pethrick, R. A. Kautsch Gummi Kunstst 1998, 51, 429.
2. Gatos, K. G.; Kameo, K.; Karger-Kocsis, J. Express Polym Lett 2007, 1, 27.
3. Tan, H.; Isayev, A. I. J Appl Polym Sci 2008, 109, 767.
4. Lai, S. M.; Liu, S. D. Polym Eng Sci 2007, 47, 77.
5. Sarkar, D.; Yang, J.-C.; Klettlinger, N.; Lopina, S. T. Express Polym Lett 2007, 1, 724.
6. Molero, C.; de Lucas, A.; Romero, F.; Rodriguez, J. F. J Appl Polym Sci 2008, 109, 617.
7. Bakare, I. O.; Pavithran, C.; Okieimen, F. E.; Pillai, C. K. S. J Appl Polym Sci 2008, 109, 3292.
8. Deng, J. N.; Cao, J.; Li, J. H.; Tan, H.; Zhang, Q.; Fu, Q. J Appl Polym Sci 2008, 108, 2023.
9. Hill, D. J. T.; Killeen, M. I.; O'Donnell, J. H.; Pomery, P. J.; St. John, D.; Whittaker, A. K. J Appl Polym Sci 1996, 61, 1757.
10. Bremner, T.; Hill, D. J. T.; Killeen, M. I.; O'Donnell, J. H.; Pomery, P. J.; St. John, D.; Whittaker, A. K. J Appl Polym Sci 1997, 65, 939.
11. Zhang, Z.; Barkoula, N. M.; Karger-Kocsis, J.; Friedrich, K. Wear 2003, 255, 708.
12. da Silva, R. C. L.; da Silva, C. H.; Medeiros, J. T. N. Wear 2007, 263, 974.
13. Karger-Kocsis, J. Kautsch Gummi Kunstst 2006, 59, 537.
14. Elleuch, R.; Elleuch, K.; Salah, B.; Zahouan, H. Mater Des 2007, 28, 824.
15. Sombatsompop, N. J Appl Polym Sci 1999, 74, 1129.
16. Wang, X. D.; Luo, X. Eur Polym J 2004, 40, 2391.
17. Wu, L.; Luo, X.; Wang, X. D. J Appl Polym Sci 2006, 102, 5472.
18. Dhamodharan, R.; Maiti, P.; Radhakrishnan, G. Polym Plast Technol Eng 2007, 46, 163.
19. Karger-Kocsis, J.; Felhös, D.; Xu, D. Wear, to appear.
20. Felhös, D.; Karger-Kocsis, J.; Xu, D. J Appl Polym Sci 2008, 108, 2840.
21. Schallamach, A. Wear 1971, 17, 301.
22. Kar, K. K.; Bhowmick, A. K. J Appl Polym Sci 1997, 64, 1541.
23. Karger-Kocsis, J.; Mousa, A.; Major, Z.; Békési, N. Wear 2008, 264, 357.